Title

p27 allosterically activates cyclin-dependent kinase 4 and antagonizes palbociclib inhibition

Journal

Science, 366(6471)

ISSN

0036-8075

Authors

Guiley, Keelan Z

Stevenson, Jack W

Lou, Kevin

et al.

Publication Date

2019-12-13

DOI

10.1126/science.aaw2106

Peer reviewed

Published in final edited form as:

Science. 2019 December 13; 366(6471): . doi:10.1126/science.aaw2106.

p27 Allosterically Activates Cyclin-Dependent Kinase 4 and Antagonizes Palbociclib Inhibition

Keelan Z. Guiley[1,2], **Jack W. Stevenson**[2], **Kevin Lou**[2], **Krister J. Barkovich**[2], **Vishnu Kumarasamy**[3], **Tilini U. Wijeratne**[1], **Katharine L. Bunch**[1], **Sarvind Tripathi**[1], **Erik S. Knudsen**[3], **Agnieszka K. Witkiewicz**[3], **Kevan M. Shokat**[2], **Seth M. Rubin**[1,*]

[1]Department of Chemistry and Biochemistry, University of California, Santa Cruz, CA 95064, USA

[2]Department of Cellular and Molecular Pharmacology and Howard Hughes Medical Institute, University of California San Francisco, San Francisco, CA 94158, USA

[3]Center for Personalized Medicine, Roswell Park Cancer Center, Buffalo, NY 14263, USA

Abstract

The p27 protein is a canonical negative regulator of cell proliferation and acts primarily by inhibiting cyclin-dependent kinases (CDKs). Under some circumstances p27 is associated with active CDK4, but no mechanism for activation has been described. We found that p27, when phosphorylated by tyrosine kinases, allosterically activated CDK4-CycD1. Structural and biochemical data revealed that binding of phosphorylated p27 (phosp27) to CDK4 altered the kinase ATP site to promote phosphorylation of the retinoblastoma tumor suppressor protein (Rb) and other substrates. Surprisingly, purified and endogenous phosp27-CDK4-CycD1 complexes were insensitive to the CDK4-targeting drug palbociclib. Palbociclib instead primarily targeted monomeric CDK4 and CDK6 (CDK4/6) in breast tumor cells. Our data characterize phosp27-CDK4-CycD1 as an active Rb kinase that is refractory to clinically relevant CDK4/6 inhibitors.

One Sentence Summary:

A kinase inhibitor and cancer drug works by an unexpected mechanism.

Cyclin-dependent kinases 4 and 6 (CDK4/6) drive cell proliferation by partnering with D-type cyclins (CycD) to phosphorylate the retinoblastoma protein (Rb). Rb is subsequently hyperphosphorylated and inactivated by CDK2 to trigger passage through G1 phase of the cell cycle (1-3). Disruption of this CDK4/6–Rb signaling pathway is ubiquitous in

*Correspondence to: srubin@ucsc.edu.

Author Contributions: K.Z.G. and S.M.R. designed the structural studies and enzyme analysis, K.Z.G., J.W.S., K.L., K.J.B, and K.M.S. designed the XO44 and palbociclib-biotin experiments, and K.Z.G., A.K.W., E.S.K., K.M.S., and S.M.R. designed the breast cancer cell experiments. K.Z.G., T.U.W., and K.L.B. purified protein. K.Z.G. crystallized protein and determined the structures with help from S.T.. K.Z.G. and S.M.R. performed enzyme and binding assays. J.W.S., K.L., and K.J.B. performed the XO44 experiments. K.L. synthesized palbociclib-biotin. K.Z.G., J.W.S., V.K. performed immunoprecipitation experiments. K.Z.G, J.W.S., A.K.W., E.S.K., K.M.S., and S.M.R. wrote the manuscript.

Competing Interests: S.M.R. and K.Z.G. filed a patent application describing an engineered p27 protein.

Data and Materials Availability:
All data and materials are publicly available. Structure factors and coordinates for the crystal structures are available in the Protein Data Bank under accession codes: 6P8E, 6P8F, 6P8G, and 6P8H.

tumors and typically occurs through overexpression of CycD1 or loss of the CDK4/6 specific inhibitor p16^{INK4a}, both of which increase CDK4/6 activity, leading to uncontrolled proliferation (4-6). Specific CDK4/6-targeting ATP-competitive drugs such as palbociclib are approved for estrogen receptor–positive breast cancer and are being tested in clinical trials for application in diverse cancer types (4, 5, 7, 8). As the use of CDK4/6 inhibitors as therapies increases, it becomes critical to understand their mechanism and factors that promote sensitivity or resistance.

CDK4/6 regulation is multilayered, reflecting the need to integrate diverse growth signals to control the cell cycle (3). Canonical CDKs require cyclin binding to properly structure their catalytic site (9). CDK4-CycD is unique in that CycD binding alone does not induce an active kinase structure (10, 11). CDK4-CycD also has relatively fewer characterized substrates and poorer catalytic activity compared to other CDKs (12-16). There are several cofactors that interact with CDK4-CycD to modulate complex activity, assembly and localization. The Rb family members (Rb, p107 and p130), which are the best-characterized substrates of CDK4, contain a specific activating interaction sequence (15, 17, 18). The Hsp90-Cdc37 chaperone complex stabilizes monomeric CDK4 by binding the unfolded N-lobe of the kinase (19, 20). The INK4 family (p19, p18, p16 and p15) inhibits CDK4/6 by obstructing cyclin binding and by pulling the activation segment (also called the T-loop) into an inactive conformation (21, 22). Activation segment phosphorylation by the CDK-activating kinase (CAK) stimulates CDK4 activity (23, 24).

CIP (p21) and KIP (p27 and p57) proteins are CDK2 inhibitors *in vitro* and in cells under conditions of growth arrest (25). They are intrinsically disordered proteins that fold onto a cyclin and then a CDK sequentially to form ternary complexes (26). Mice lacking p21 or p27 are susceptible to tumorigenesis (27, 28), which is consistent with the important roles of CIP and KIP proteins in negatively regulating the cell cycle through CDK2 inhibition. p27 degradation is critical for licensing entry into S phase, and p21 is a key effector of p53-activated senescence (25, 29). p27 directly inhibits CDK2-CycA by occluding a substrate-docking site and by inserting a small helix within the p27 CDK-inhibitory domain into the CDK2 ATP site (30).

p21 and p27 have a more complex role in regulating CDK4. Although they can inhibit CDK4 under some conditions, they are also necessary for CDK4 activity. Embryonic fibroblasts that lack both p21 and p27 fail to assemble active CDK4-CycD complexes (31). Much of p27 is found in a complex with CDK4-CycD in proliferating cells, and active CDK4 complexes in cells contain both CycD and p27 (25, 32-36). While high levels of p21 are inhibitory, low levels induce assembly and nuclear localization of enzymatically active CDK4 complexes (37). The activity of CDK4 complexes requires phosphorylation of p27 by non-receptor tyrosine kinases (NRTKs) (34, 35, 38), including the breast tumor kinase Brk (also called PTK6). However, it is unclear whether and how p21 and p27 directly stimulate CDK4 catalytic activity, how this activation is mediated by p27 phosphorylation, and how p27 influences CDK4's sensitivity to chemical inhibitors such as palbociclib.

Crystal structures of p21-CDK4-CycD1 and p27-CDK4-CycD1 complexes

To better understand p21 and p27 regulation of CDK4, we determined the crystal structures of p21-CDK4-CycD1 and p27-CDK4-CycD1 complexes at 3.2 Å and 2.3 Å resolution, respectively (Fig. 1 and Tables S1 and S2). p21 and p27 similarly fold into a single helix that spans CDK4-CycD1. The structures demonstrate why both proteins function as assembly factors. p21 and p27 contain a subdomain 1 (D1), which docks into a hydrophobic cleft in CycD1, and a subdomain 2 (D2), which binds the N-lobe of CDK4 (Fig. 1 and Fig. 2). CDK4 and CycD1 are joined through the bridging helix (α1), which provides a rigid constraint to define the relative orientation of the cyclin and kinase N-lobe domains (Fig. 1, A and B).

The trimer structures demonstrate two key mechanisms of inhibition. First, p21 and p27 use their RxLF motif in D1 to block access to a critical substrate-docking site on CycD (Fig. 2, A and B) (39, 40). Similar D1 domain-mediated interactions are also observed between p27 and CDK2-CycA (Fig. S1, A and B). In a second inhibitory mechanism, the p21 and p27 D2 domains displace the first strand (β1) of the CDK4 N-lobe β-sheet (Fig. 2C). As a result, the glycine rich loop (Gly-loop; residues 13-19 in CDK4) is dislodged from the CDK4 active site and the ATP-binding pocket is disrupted. A striking difference in how p27 binds CDK2 and CDK4 was observed in the interaction between p27 D2 and the kinase domain. Whereas p27 inserts a small 3_{10}-helix into the CDK2 ATP site (30), a 3_{10}-helix was not observed at the corresponding location in CDK4 (Fig. 2D and Fig. S1C). Differences in the CDK4 hinge region from CDK2 suggest that 3_{10}-helix insertion of p27 into the CDK4 active site would be sterically hindered (Fig. S1D).

p21 and p27 binding rotates the CDK4 N-lobe and releases the kinase activation segment

We compared the trimer structures to the known CDK4-CycD dimer structures (10, 11). Unexpectedly, p21 and p27 induced structural changes that better shape the active site for catalysis. p27 binding rotated the N-lobe of CDK4 toward CycD1 (Fig. 3, A **through** D). The strands in the N-lobe β-sheet were shifted by ~4-6 Å such that β-strand 2 (β2) of the trimer complex replaced the β-strand 3 (β3) position of the dimer, β3 replaced β5, and β5 replaced β4. An important consequence of this altered N-lobe conformation is that the activation segment was released from the CDK4 active site, because specific interactions between β3 and β5 and the activation segment helix were broken (Fig. 3B). The release represents an important step that allows substrate binding in the kinase active site (41). For CDK1 and CDK2, activation segment release occurs upon binding to a cognate cyclin, and phosphorylation of the activation segment by CAK further improves substrate binding (42). However, in the crystal structure of the CDK4-CycD1 dimer, the activation segment remains in a substrate-blocking conformation despite the introduction of a phosphomimetic (T172D) at the CAK phosphorylation site (Fig. 3B) (10). The release of the activation segment observed upon p27 binding (Fig. 3B) is a unique mechanism to CDK4 and likely explains the requirement of p27 for CDK4 activation segment phosphorylation by CAK (24).

A second result of the β-sheet rearrangement was that the catalytic lysine (K35) on β3 was pulled into a position to accept the β- and γ- phosphates of ATP (Fig. 3, C and D). This position of K35 is similar to that of the corresponding catalytic lysine (K33) in active CDK2-CycA (Fig. S1E) (9, 30). In contrast, the position of K35 in the CDK4-CycD1 dimer is similar to its position in the inactive CDK2 monomer structure (10, 11). This conformational change in the N-lobe does not occur when p27 binds CDK2 and is therefore an allosteric activating mechanism of p27 specific to CDK4 (Fig. S1, A and F) (30).

While the p21 and p27 trimer complexes are primed for catalysis in that K35 is positioned to coordinate ATP and the activation segment is released, there are still aspects of the structure that indicate additional activating mechanisms are required. The D2 domain must be displaced to permit formation of the ATP-binding G-loop. In addition, comparison of the CDK4 trimer structure with an active CDK2 structure indicates that the C-helix (also known as the PSTAIRE helix) in CDK4 remains in an inactive position, with its critical catalytic glutamate pointing away from the active site (Fig. 2C and Fig. 3D). We propose that the structure determined here is an intermediate along a pathway to activation and that substrate binding, ATP binding, or activation segment phosphorylation in conjunction with p27 binding may induce the required rotation of the C-helix (Fig. S2A).

Tyrosine phosphorylation of p27 but not p21 activates CDK4 trimer complexes

To quantify the kinase activity of p21- and p27-CDK4-CycD1, we assayed activity of recombinant CDK4 complexes (Fig. 3, E **through** G). We used a phosphorylation site mimetic in the CDK4 activation segment (CDK4 T172E), because there was heterogeneity in phosphorylation of the T172 site in our purified protein (Fig. S2, B and C). We tested the CDK4-CycD1 dimer (called K4D1/-, because it lacks p21 or p27), the trimer with p21 or p27 (K4D1/p21 or K4D1/p27), and the trimer with tyrosine kinase (Brk/PTK6) phosphorylated p21 and p27 (K4D1/phosp21 or K4D1/phosp27) (Fig. 3E and Fig. S3). The dimer demonstrated strong activity toward the purified Rb C-terminal domain (residues 771-928, $Rb^{771\text{-}928}$), whereas the trimer with unphosphorylated p21 or unphosphorylated p27 demonstrated poor activity. Consistent with observations in cell culture (34, 35), tyrosine phosphorylation of p27 restored its recombinant trimer enzyme activity. The tyrosine kinase phosphorylated p21 had only slight additional activity, indicating that p21 trimer complexes are mostly inhibited despite tyrosine phosphorylation.

We focused on the strong activity of the phosphorylated p27 trimer and used steady-state kinetic experiments to quantify enzyme processing of ATP (Fig. 3, F and G, and Fig. S4). We tested CDK4 activity of the dimer and the phosp27-trimer complex toward $Rb^{771\text{-}928}$, $Rb^{771\text{-}874}$ [residues 771-784; this shorter Rb fragment lacks a CDK4 docking sequence (15, 17, 18)], $Cdc6^{1\text{-}119}$ (residues 1-119, a CDK4 substrate that contains an RxLF docking sequence) (13), and $p107^{949\text{-}1068}$ (residues 949-1068, which lacks any known docking sequence). In the case of all four substrates, the K_M of ATP for the K4D1/phosp27 trimer was reduced compared to that of K4D1/- and was more similar to the K_M of CDK2 and that of most serine/threonine kinases (16). This decrease in K_M, which we also observed for

CDK6-CycD1 but not for CDK2-CycA (Fig. S5), is consistent with our structural results that p27 binding induces an N-lobe conformation in CDK4 that supports ATP coordination. We note that although we observed activity from reconstituted phosp27-CDK6-CycD1 trimers *in vitro*, it is unclear whether these complexes exist in cycling cells (43).

In the activity assays, phosp27 also had an inhibitory effect that is specific for substrates containing a CDK docking sequence. When assaying the K4D1/- dimer, the ATP V_{max} and the Rb substrate k_{cat}/K_M both decreased upon deletion of the docking sequence in Rb (compare $Rb^{771\text{-}928}$ to $Rb^{771\text{-}874}$), supporting the importance of docking in dimer phosphorylation of Rb (Fig. 3G and S4B) (17, 18). The ATP V_{max} decreased upon addition of phosp27 when assaying $Rb^{771\text{-}928}$ (13-fold decrease) and $Cdc6^{1\text{-}119}$ (4-fold decrease), which both contain docking sequences (Fig. 3G). In contrast, the ATP V_{max} only modestly decreased for $p107^{949\text{-}1068}$ and for $Rb^{771\text{-}874}$, which lack docking sequences. The $Rb^{771\text{-}928}$ substrate k_{cat}/K_M but not the $Rb^{771\text{-}874}$ substrate k_{cat}/K_M decreased upon addition of p27 (Fig. S4B), and the kinetics of the trimer activity toward both Rb substrates were similar (Fig. 3G). These observations indicate that even in the active complex, p27 inhibits CDK4 activity toward some substrates by occluding the docking site in CycD (Fig. 2A).

Structural mechanism of p27-CDK4-CycD activation by tyrosine phosphorylation

We solved the structure of a phosp27-CDK4-CycD1 complex to determine how tyrosine phosphorylation relieves p27 inhibition (Table S1). Y74 was in a similar position to that in the unphosphorylated trimer, but there was clear electron density for the phosphate (Fig. 4, A and B, and Fig. S6). Y74 is part of an aromatic cluster in p27 D2 that binds the CDK4 N-lobe. The structural data predict that Y74 phosphorylation would weaken this association by destabilizing the hydrophobic interface between Y74 and the N-lobe of CDK4 (Fig. 4, A and B). In p21, a phenylalanine (F62) is in the position of Y74 in p27 such that the p21 D2 domain would remain bound without the addition of a phosphate (Fig. 1C and Fig. 4C).

In a structure we solved of the trimer containing p27 with phosphomimetics (Table S1), temperature B-factors were ~10 to 20 $Å^2$ higher for sidechains in the aromatic cluster in D2 and the electron density was weaker around W60 and E74 (Fig. S6). The higher B-factors and weaker density are consistent with lower D2 occupancy and higher disorder. Deletion of the D2 domain from p27 or mutation of the tyrosines to glutamate phosphomimetics generated a trimer complex that phosphorylated $Rb^{771\text{-}928}$ (Fig. 4D and Fig. S7). Solution studies with p27 binding to CDK2-CycA demonstrate that phosphorylation of Y74 results in loss of interactions between the D2 domain of p27 and the N-lobe of CycA (44). Together these results support a model in which phosphorylation or phosphomimetics weaken the affinity of the D2 domain for CDK4 N-lobe, allowing for the formation of the Gly-loop and activation of the kinase. The activation segment was not homogeneously phosphorylated in our structure (Fig. S2B), so we cannot rule out that activation segment phosphorylation and the ultimate repositioning of the C-helix also plays a role in removing the D2 domain from the N-lobe.

Y88 and Y89 were disordered in all the p27-CDK4-CycD1 crystal structures, and the CDK4 trimer assembled with p27 containing a phosphomimetic at Y74 had similar though slightly less activity to that of the enzyme assembled with phosphomimetics at all the tyrosines (Fig. 4D). Thus, Y74 phosphorylation appeared to be nearly sufficient for p27 activation of CDK4, although the data indicate that there may have been some contribution from Y88/Y89 phosphomimetics in the p27 triple glutamate mutant (Fig. 4D). This mechanism for turning off p27 inhibition is different from the mechanism in CDK2, in which phosphorylation of p27 Y88 and Y89 are necessary for ejection of a p27 3_{10} helix from the catalytic site (Fig. S1C) (45). These phosphorylation sites in p27 and the corresponding site in p21 (Y77) are located in a sequence that remains disordered upon CDK4 binding (Fig. 1C), which is consistent with their weaker role in the mechanism of CDK4 activation. The more important role of the Y74 phosphorylation site also explains the observed poor activity of Brk-phosphorylated p21 complexes (Fig. 3E), as p21 lacks a tyrosine at the equivalent position of Y74 in p27 (Fig. 1C and Fig. 4C). We conclude that while p21, like p27, primes CDK4 for catalysis by releasing the activation segment, p21 tyrosine phosphorylation does not relieve D2 inhibition, and the complex remains mostly inhibited.

p27-CDK4-CycD1 complexes are insensitive to CDK4/6-specific inhibitors

The structural changes in the kinase N-lobe that are induced by p27 binding indicate that palbociclib-type inhibitors should have poor potency toward active CDK4 trimer complexes (Fig. 5A). The “gatekeeper” residue Phe93 in β5 and also Ala33 in β3 are rotated away from making contacts with the C5-methyl and C6-acetyl groups in the pyridopyrimidine scaffold of palbociclib (46, 47). We tested the effects of palbociclib, ribociclib, and abemaciclib on activity of the reconstituted CDK4 enzyme complexes (Fig. 5B and Fig. S8A). All three compounds inhibited $Rb^{771\text{-}928}$ phosphorylation by CDK4-CycD1 dimer (K4D1/−) as expected; however, the active phosp27-CDK4-CycD1 trimer (K4D1/phosp27) was relatively insensitive to the drugs, with apparent inhibition constants ~10 μM or higher. We measured the binding affinity of palbociclib for CDK4 complexes by isothermal titration calorimetry (ITC). The drug only bound CDK4 monomer and K4D1/- dimer tightly. Consistent with our structural and kinetic data, we detected no affinity for K4D1/phosp27 trimer (Fig. 5C and Fig. S8B). We also measured binding of p27 to CDK4 monomer and found no affinity if the enzyme was first saturated with palbociclib (Fig. 5C and Fig. S8C). These data demonstrate that binding of p27 and palbociclib to CDK4 are mutually exclusive.

Palbociclib does not inhibit endogenous CDK4 activity

We tested whether the activity of endogenous cellular CDK4 complexes is inhibited by palbociclib. We immunoprecipitated p27 complexes from MCF7, MDA-MB-231, and T98G cells. MCF7 and MDA-MB-231 cells are Rb-positive and palbociclib-sensitive breast cancer cells that differ in estrogen receptor (ER) status (46). T98G cells are Rb (+) and ER (−) glioma cells that are relatively less sensitive to palbociclib (see below, Fig. 8A). The immunoprecipitates phosphorylated purified $Rb^{771\text{-}928}$ in the ^{32}P-ATP assay; however, the activity was insensitive to palbociclib that was added to the kinase reactions (Fig. 5D). We considered that this palbociclib-insensitive activity might be from CDK2. While it is thought that cellular CDK2 complexes with p27 are not active (32), we found that

reconstituted K2A/phosp27 complexes phosphorylated Rb (Fig. S5C). However, the p27 immunoprecipitate activity was also not inhibited by the CDK2 inhibitor dinaciclib, and therefore the immunoprecipitate likely contained a CDK4 activity and not a CDK2 activity (Fig. S9).

To test the entire cellular pool of CDK4 activity, we immunoprecipitated CDK4 from the same cell lines using an antiserum raised against the CDK4 C-terminus, which contains a sequence distinct from CDK2 (48). Palbociclib also poorly inhibited the immunoprecipitated CDK4 kinase activity (Fig. 5E), which is consistent with previous observations that CDK4 activity mostly arises from trimer complexes (25, 31-37) and our observation that trimer is insensitive to drug (Fig. 5B).

An ATP-site occupancy probe targets CDK4 monomers in cells

To examine the association of an inhibitor with endogenous CDK4 complexes, we treated MCF7 and MDA-MB-231 cells with the covalent ATP-site occupancy probe XO44 (49). XO44 labeled both CDK4 and CDK2 in these cells and could be detected by a gel shift upon coupling to an analysis probe (Fig. 6A and Fig. S10, A and B). While XO44 labeled most CDK2 and the mitotic kinase Aurora B (Fig. S10A), it labeled only ~40 to 60% of CDK4 even at high concentrations, indicating that a resistant population of the protein exists. CDK4 labeling in cells was inhibited by palbociclib (Fig. 6B and Fig. S10C), demonstrating that XO44 and palbociclib bind the ATP site competitively and that the population of CDK4 that is targeted by XO44 is also targeted by palbociclib-type inhibitors. XO44 labeled recombinant CDK4 efficiently in dimer complexes but not in unphosphorylated or phosphorylated trimer complexes (Fig. 6C).

We treated cells with XO44 and palbociclib and fractionated the lysates with size-exclusion chromatography (Fig. 6D and S10D). We observed CDK4 in high-molecular-size fractions co-migrating with Hsp90 and Cdc37 (e.g. fractions 5 and 6), in mid-size fractions with CycD1 and p27 (fractions 9 and 10), and in low-size fractions that likely contain monomers (fractions 15 and 16) (34, 36). Consistent with ATP-competitive probes sequestering obligate Hsp90-client kinases from the chaperone system (50, 51), we observed a reduction in the abundance of large-sized, putatively Hsp90/Cdc37-bound CDK4 in extracts from XO44- and palbociclib-treated cells. We also detected greater quantities of CDK4 in small-sized monomer fractions upon treatment with either compound, and only the CDK4 population observed in these fractions was labeled with XO44 (Fig. 6D, fractions 15 and 16, XO-44 + click). Considering that CDK4 inhibitors do not associate with CDK4 bound by INK proteins (52), we propose that the tested inhibitors primarily bind CDK4 monomers in cells and increase the abundance of the inactive monomer population.

We synthesized a palbociclib analog linked to biotin, and we used it to precipitate CDK4/6 from cell extracts to determine which proteins exist in the complexes targeted by palbociclib-type inhibitors (Fig. 7A). Consistent with our activity and ITC binding assays, the palbociclib-biotin precipitated recombinant CDK4-CycD1 dimer but not recombinant p27-CDK4-CycD1 trimer (Fig. 7B). Strikingly, in breast cancer cell lysates, the palbociclib-biotin strongly precipitated CDK4 and CDK6, but did not precipitate any detectable p21 or

p27 (Fig. 7, C and D). This observation demonstrates further that the drug does not bind trimer complexes with p21 and p27 in these cells. A faint band reproducibly appeared in the CycD1 blot, indicating that there may be some small population of dimer complexes targeted by the drug. However, we conclude that monomer CDK4 and CDK6 are the predominant targets of palbociclib in these cells.

Palbociclib-induced cell-cycle arrest coincides with loss of CDK2 and not CDK4 activity

We treated cells with palbociclib for 48 hrs, which, similar to previous descriptions, lead to strong arrest of the breast cancer cells and to weaker arrest of T98G cells as determined by EdU incorporation and propidium iodide staining (53, 54) (Fig. 8A and Fig. S11). Endogenous CDK4 and CycD1 complexes retained kinase activity despite the cells arresting with drug treatment (Fig. 8B and S12A). This similar activity in palbociclib-treated cells was observed despite increased levels of CycD1 (Fig. 8C and Fig. S12B) (53). In contrast, CDK4 complexes immunoprecipitated from serum-starved NIH/3T3 cells lack Rb-directed kinase activity (Fig. S12C), and the lack of activity coincides with reduced CycD1 levels. In the cycling breast cancer cells tested, we did not observe palbociclib inhibiting CDK4- or CycD1-associated kinase activity, which is consistent with the lack of susceptible dimer complexes that could be detected in their lysates (Fig. 6D and Fig. 7, C and D).

Unlike CDK4 complexes, CDK2 complexes immunoprecipitated from the breast cancer cells had diminished activity following 48-hr palbociclib treatment (Fig. 8B). CDK2 inhibition at this drug concentration is likely indirect (5, 46), resulting at least in part from lower levels of CycA (Fig. 8C) (53). We also observed evidence for an increase in p21 but not p27 in CDK2-CycE complexes (Fig. 8, C and D and Fig. S12, D and E). In reciprocal co-immunoprecipitation experiments, additional p21-CycE association was detected after 48 hrs. We could not detect p27 in the CycE1 IP either without or with palbociclib treatment, so we cannot determine whether p27 also plays a role in down-regulating the CDK2-CycE activity. We conclude that palbociclib treatment indirectly leads to CDK2 inhibition and that this CDK2 inhibition, and not CDK4 inhibition, correlates with cell-cycle arrest.

Discussion

CIP/KIP proteins were first characterized as CDK inhibitors, particularly as potent inhibitors of CDK2-CycA/E (25, 55-59). In contrast, other evidence implicated non-inhibitory roles for p21 and p27 in mediating CDK4-CycD function, including complex assembly and nuclear localization (31, 37). Moreover, the observations that active CDK4-CycD tolerated the presence of p27 and that Rb-directed kinase activity in cells contained p27 led to models that CDK4-CycD may titrate inhibitory p27 away from CDK2 (25, 33, 37, 60). Our data demonstrate that p27 is not merely a non-inhibitor, but it in fact allosterically activates CDK4-CycD, remodeling the kinase to increase the catalytic efficiency of ATP processing. Our structural data demonstrate that this effect is specific to CDK4 (vs. CDK2) and is primarily induced by Y74 phosphorylation in p27. While p21 also acts as an assembly factor for active CDK4-CycD1 (31), p21 contains a phenylalanine at the equivalent position as Y74 (Fig. 1C and 4C), and p21 trimer complexes cannot be activated by D2 displacement as

in p27. As a result, phosphorylated p21 trimer complexes have relatively less activity than phosphorylated p27 complexes.

The catalytic efficiency of the phosp27-CDK4-CycD1 trimer was greater than the catalytic efficiency of the dimer for most of the substrates we investigated (Fig. 3G). The requirement of p27 for efficient phosphorylation may explain why, relative to CDK2 for example, fewer cell-cycle substrates have been identified for CDK4/6 and why it has been thought that Rb is a preferred CDK4/6 substrate (12, 14, 15, 17, 18). Additional CDK4/6 substrates have been identified more recently (13, 61, 62), and it will be important to explore the role of p27 in their regulation by CDK4/6 phosphorylation. Our observation that the CDK4-CycD1 dimer catalytic efficiency was dependent on the last ~50 amino acids of Rb is consistent with reports of a CDK4 docking site in the Rb C-terminal domain (17, 18). Docking allows Rb to more tightly associate with the dimer and be phosphorylated even when ATP affinity is so low. In contrast, we observed that the trimer activity did not depend on a substrate docking sequence, suggesting that a role of p27 activation may be to broaden CDK4 substrate specificity. Our data also implicate a competitive association between Rb and p27 for CDK4-CycD and indicate that p27 still functions to temper Rb-directed CDK4 activity even in the context of active trimer complexes.

CDK4/6-specific inhibitors were developed through optimizing potency and selectivity toward CDK4-CycD dimer, despite evidence that the physiological complex contains CIP or KIP family inhibitors such as p27 (25, 31-37, 46). Our data demonstrate that active recombinant CDK4 complexes containing p27 are not sensitive to these inhibitors and that palbociclib does not associate with active endogenous p27 trimer complexes. Moreover, we did not detect inhibition of CDK4 activity in drug-arrested breast cancer cells, and we did not robustly detect CDK4-CycD1 dimer complexes in cell lysates. Still, we recognize that dimer inhibition may occur in some contexts and that some small population of dimer may be targeted even in the breast cancer cells tested here. In light of the differences between dimer and trimer response to CDK4/6 palbociclib-type inhibitors *in vitro*, it will be important to explore how the balance of dimer and trimer complexes may influence sensitivity to drugs in cells or *in vivo*.

Our data implicate an additional mechanism toward cell-cycle arrest in which palbociclib associates with CDK4 monomer instead of binding and inhibiting CDK4 dimer or trimer activity. One outcome is that the population of CDK4 monomer increases, and it is possible that this CDK4-palbociclib complex is recognized and induces a response, such as the decrease in CycA abundance (53) or an increase of p21 in CDK2-CycE complexes. Both of these outcomes correlate with our observed lower CDK2 activity. A reported CDK4/6 degrader drug is not as effective as palbociclib in inhibiting Rb phosphorylation (63), and, a recent study finds that cells expressing a catalytically inactive CDK4 are arrested when treated with palbociclib (64). These results perhaps reflect the fact that palbociclib-induced cell-cycle arrest does not require inhibition of CDK4 activity but alternatively results from indirect inhibition of CDK2. This indirect role of CDK4 in modulating CDK2 activity is consistent with observations that CDK4-CycD expression can activate CDK2 through sequestration of p27 and without the requirement of CDK4 catalytic activity (25, 59).

We note the similarity of this mechanism of palbociclib inhibition with that of the p16-INK family of CDK4 protein inhibitors, which sequester inactive monomer CDK4 (Fig. 8E). The ability of palbociclib to mimic p16 may in part explain why cells lacking p16 are often most sensitive to palbociclib-type inhibitors (53, 54, 65, 66). We suggest that, similarly to the downstream effects of p16, accumulation of CDK4 monomer upon palbociclib treatment indirectly lowers CDK2 activity, potentially through the shuttling of p21 to CDK2 complexes (25, 36, 67, 68). In cycling cells, this drug-induced reorganization of CDK complexes may occur when p21 is re-synthesized following its degradation before S phase and/or when CycD1 is low in S phase and would lead to cell-cycle arrest (69). The targeting of an inactive kinase, rather than inhibition of assembled kinase activity, may apply to other kinase therapeutic targets as well (70), and we note that Gleevec similarly inhibits an inactive confirmation of the Abl kinase (71).

Materials and Methods:

Recombinant protein expression

Full-length human CDK4, CDK6, cycD1, p21, p27, and Brk were expressed and purified from Sf9 cells. CDK4, CDK6, p21, p27, and Brk were expressed as GST fusion proteins. CycD1 was co-expressed with other components untagged or, where indicated, with a Strep tag. Lysates were first purified by GS4B affinity chromatography. Proteins were then eluted from the resin and subject to Source 15Q (GE Healthcare) anion exchange chromatography. The elution fraction was then subjected to TEV protease cleavage overnight in 25 mM Tris pH 8.0, 200 mM NaCl, 1 mM DTT, 0.5 mM EDTA. The protein was then passed over GS4B affinity resin again to remove free GST, concentrated, and stored in a buffer containing 20 mM Tris pH 8.0, 200 mM NaCl, 1 mM DTT, and 20% glycerol. CDK2-CycA was expressed in *E. coli* and purified as previously described (72).

Phosphorylation of p21 and p27

Recombinant p21 and p27 were expressed as a GST fusion in *E. coli* and purified as described above. Purified proteins were treated with 10% GST-Brk (by mass) in a buffer containing 50 mM Tris pH 8.0, 150 mM NaCl, 1 mM DTT, 10 mM $MgCl_2$ and 1 mM ATP and incubated at 4°C for 24 hours. The phosphorylated p21 or p27 were purified by passing through GS4B affinity resin and eluted from a Superdex 75 column (GE Healthcare) in a buffer containing 25 mM Tris pH 8.0, 100 mM NaCl, and 1 mM DTT. The extent of phosphorylation was confirmed using electrospray mass spectrometry on a SCIEX X500 QTOF spectrometer.

Crystallization, data collection, structure determination, and model refinement

For crystallization, human CDK4 (residues 1-303, (ΔG45-G47, G43E, G44E), truncated cycD1 (16-267), p27 kinase-inhibitory domain ($p27^{KID}$; 25-93), and the p21 kinase-inhibitory domain ($p21^{KID}$; 14-81) were prepared as described above. The CDK4 contains mutations in a glycine-rich sequence that mimic CDK6 and were required for crystallization (10, 11). The CDK4 complexes were prepared for crystallization by elution from a Superdex 200 column (GE Healthcare) in a buffer containing 10 mM Tris pH 8.0, 100 mM NaCl, and 1 mM DTT. The p27-CDK4-CycD1, p27(3E)-CDK4-CycD1, and p21-CDK4-CycD1

complexes were crystallized from an 10 mg/mL solution by microbatch method under Al's oil at 22°C. Rods formed after three days in 100 mM Tris, 10% PEG 8000, and 200 mM $MgCl_2$, pH 7.0. Crystals were cryo-protected in reservoir solution supplemented with 25% glycerol and cryo-cooled in liquid nitrogen.

The phosp27-CDK4-CycD1 complex was prepared for crystallization by mixing 3:1 molar ratio of phosphorylated p27 and CDK4-CycD1 dimer followed by elution from a Superdex 200 column in a buffer containing 10 mM Tris, 100 mM NaCl, and 1 mM DTT, pH 8.0. The complex was crystallized from an 10 mg/mL solution by sitting drop vapor diffusion method at 22°C. Rods formed after three days in 100 mM Tris, 17% PEG 3350, 100 mM $CaCl_2$ and 10 mM $MgCl_2$ pH 7.0. Crystals were cryo-cooled in the reservoir solution supplemented with 25% glycerol.

Data were collected at the Advanced Light Source, Laurence Berkeley National Laboratory at beamline 8.3.1. Diffraction spots were integrated using MOSFLM (73), and data were merged and scaled using Scala in the CCP4 software package (74, 75). The structure of the p27-CDK4-CycD1 trimer was first determined by molecular replacement using Phaser and the CDK4-CycD1 dimer as a search model (PDB ID: 2W9F) (76). A model for p27 was then built into the extra electron density with Coot (77), and the model was refined with Phenix (78). Models for the CDK4-CycD1 trimer complexes containing phosp27, p27(3E), or p21 were then built and refined starting from the unphosphorylated p27 structure.

Western blots and antibodies

Details on the antibodies used and the procedures for Western blotting can be found in the Supplementary Materials.

Kinase assays

Recombinant CDK4 (0.5 μM), CDK2 (0.5 μM), or CDK6 (1 μM) complexes were mixed with substrate (30 μM) in a kinase buffer containing 25 mM Tris pH 8.0, 200 mM NaCl, 10 mM $MgCl_2$, 1 mM DTT, 250 μM ATP (or as indicated), and 100 μCi of ^{32}P-γ-ATP. Substrate was diluted into the reaction buffer, and the reaction was initiated by addition of ATP. Reactions were quenched after 30 min by addition of SDS-PAGE loading buffer. Independent time-course experiments confirmed that phosphate addition is still linear with time beyond 45 min using our experimental conditions. SDS-PAGE gels were imaged with a Typhoon scanner and bands quantified using the ImageJ software package. For each assay, three replicates were performed. We note that our measured K_i values for the inhibitors on K4D1/- (Fig. 5B and Fig. S8A) are consistent with our ITC-measured K_d value for palbociclib (Fig. 5C) but are higher than IC_{50} values previously reported (4, 7, 46). We believe the difference is due to the higher ATP concentration in our assay, which we chose to be closer to the ATP K_M for K4D1/−.

For the activity assays using immunoprecipitation of endogenous CDK4, CDK2, or p27 complexes, 1 mg of whole-cell extract was immunoprecipitated with 2 μg anti-p27 antibody (SCBT DCS-72), 2 μg anti-CDK2 antibody (SCBT D-12), or 20 uL of CDK4 antiserum to C-terminal peptide (gift of Charles Sherr, St. Jude Children's Research Hospital) (48) and 25 μL protein A/G PLUS beads (SCBT) for 2 hr at 4°C. The beads were then washed 3 times

with 50 mM Tris pH 7, 150 mM NaCl, 1 mM DTT, and 5% glycerol. The final wash was performed in kinase buffer and the reaction was performed with the recombinant substrate while the enzyme complexes were on the beads.

For the activity assays using immunoprecipitated CycD1 complexes, MCF7 cells were lysed with lysis buffer containing 50 mM Tris-HCl pH 7.5, 150 mM NaCl, 0.1% NP-40, 10 mM DTT, 10% glycerol, 1X Halt protease inhibitor (Thermo Fisher), and 1 mM PMSF. 5 μg of anti-CycD1 (Invitrogen; MA5-12707) was incubated with 300 μg of the lysate overnight at 4°C. Normal mouse IgG1 (Cell Signaling Technology, 5415) was used as a control. Protein G agarose-beads were added to each IP samples and incubated up to 4 hour at 4°C. Protein immunocomplexes were washed 3 times with the lysis buffer and 2 times with kinase reaction buffer (50 mM HEPES-KOH pH 7.5, 20 mM $MgCl_2$ 1 mM DTT). Kinase reactions were carried out in 100 μl of kinase buffer in the presence of 2 mM ATP and 0.5 μg of recombinant Rb C-terminal domain as substrate by gently shaking at room temperature up to 1 hour. The resulting phosphorylated Rb protein was detected by western blotting using anti-p-Rb (S780) antibody (Cell Signaling Technology, 9307L).

Activity assays with immunoprecipitated CycE1 complexes were performed similarly, but the lysis buffer contained 50 mM HEPES-KOH pH 7.5, 150 mM NaCl, 1 mM EDTA, 1mM DTT, 0.1% Tween-20, 1X Halt protease inhibitor (Thermo Fisher), and 1 mM PMSF. Immunoprecipitation was performed with an anti-CycE1 antibody (Santa Cruz Biotechnology; SC-377100) as described for CycD1. The kinase reactions were performed in 100 μl of kinase buffer (40 mM Tris-HCl pH 8.0, 20 mM $MgCl_2$, 0.1 mg/mL BSA, 50 μM DTT) in the presence of 2 mM ATP and 0.5 μg of Rb protein as substrate by gently shaking at room temperature up to 1 hour. The resulting phosphorylated Rb protein was detected by western blotting using anti-p-Rb (S807/S811) antibody (Cell Signaling Technology, 8516S).

XO44 labeling assays

XO44 labeling was carried out as previously described (49) with some modifications. Live adherent cells were labeled by incubation with 2 μM XO44 at 37˚C for 30 min. Cells grown in 15-cm dish format to be analyzed by gel filtration were harvested as described below. Cells grown in 6-well plate format (seeded at 500,000 cells/well and allowed to recover for ~20 hr) to be analyzed by western blot were then washed twice with cold PBS, perturbed and lysed in place with 80 μL lysis buffer containing 100 mM HEPES pH 7.5, 150 mM NaCl, 0.1% NP-40, 1x cOmplete EDTA-free protease inhibitor cocktail and 1x PhosSTOP phosphatase inhibitor cocktail (both Roche). Lysates were clarified by centrifuging at 20,000 g for 20 min, then normalized to 2.5 mg/mL protein concentration using the Pierce Rapid Gold BCA assay (Thermo). 20.75 μL of lysate was treated with 4.25 μL of a master mix to give final concentrations of 1% SDS, 50 μM TAMRA-azide (in DMSO), 1 mM TCEP, 100 μM TBTA (in 1:4 DMSO:t-butyl alcohol) and 1 mM $CuSO_4$. The resulting mixture was incubated at room temperature for 1 hr before being quenched with 5 μL 6X SDS loading buffer and analyzed by western blot as described above. The TAMRA dye was used to add mass to XO44-labelled CDK4, so the XO44 modification is observable as a gel shift by using SDS-PAGE.

Gel filtration assay

Gel filtration assays on crude cell lysates were performed as previously described with modifications (36). Cells were seeded on 15-cm dishes at 10 million cells per dish and allowed to recover for ~20 hr before treatment with compounds as indicated and harvesting by washing with PBS followed by trypsinizing, pelleting and two further washes with cold PBS. Pellets of ~25 million cells were lysed in buffer containing 50 mM Tris pH 7.5, 150 mM NaCl, 1% NP-40, 10% glycerol, 1 mM EDTA plus cOmplete EDTA-free protease inhibitor cocktail (Roche) on ice for 20 min. Lysates were then clarified by centrifuging at 18,000 x g for 2×15 min. 500 μL (5 mg) of lysate was incubated with DNase I (NEB, 1 unit/mg lysate) in 1x DNase 1 reaction buffer (NEB) for 20 min on ice and briefly clarified again by centrifuging for 5 min. Samples were then loaded on a Superdex200 Increase 10/300 GL column pre-equilibrated in 50 mM HEPES pH 7.5, 150 mM NaCl, 1% NP-40, 10% glycerol. The column was eluted for 1.25 column volumes at 0.35 mL/min and 0.5-mL fractions were collected starting at 5 mL. Fractions 10-26 were analyzed by western blot as described above. Samples of fractions from XO44-treated cells were used in click reactions as described above. To benchmark purified protein complexes, 0.8 μg of p27-CDK4-CycD1 trimer was diluted in 500 μL HEPES buffer for loading. Gel filtration and western blot analysis were performed as described above.

LC-MS analysis of CDK4 covalent labeling

Recombinant purified protein complexes (1 μM) were suspended in a buffer containing 20 mM HEPES, 150 mM NaCl, and 1 mM $MgCl_2$, pH 7.5, and treated with XO44 (10 μM) or DMSO (1 % (v/v) DMSO final). After 30 min at room temperature, reactions were stopped by the addition of 10% (v/v) formic acid to a final concentration of 2% (v/v) formic acid. The extent of covalent labeling was assessed by LC-MS (Waters Xevo G2-XS QTof, ACQUITY UPLC Protein BEH C4 Column, 300Å, 1.7 μm, 2.1 mm X 50 mm). Deconvolution of multiply charged ions was performed using Waters MassLynx software (version 4.1).

Palbociclib-biotin

Details of the synthesis and characterization of palbo-biotin can be found in the Supplementary Materials.

For palbo-biotin precipitations, 100 μM palbo-biotin was first incubated with streptactin beads in PBS for 30 minutes at room temperature. The beads were then washed 3X with PBS and resuspended in 1 mg of cell extract in 50 mM HEPES pH 7.0, 150 mM NaCl, 0.1% Tween-20, 1 mM DTT, 5% glycerol, 1x cOmplete EDTA-free protease inhibitor cocktail and incubated at 4°C for 2 hours. Complexes bound to streptactin beads were eluted using 2X SDS buffer and subjected to immunoblot analysis. For recombinant protein the same protocol was followed except 2 μg recombinant protein was added to the beads in IP buffer with 1% BSA. 10 μM excess free palbociclib was added to the extract or purified proteins where indicated.

Isothermal Titration Calorimetry

Equilibrium dissociation constants were obtained using a Micro Cal VP-ITC at 15°C. For drug binding experiments, 40 μM purified CDK4-CycD1, phosp27($p27^{KID}$; 25-93)-CDK4-CycD1, and GST-CDK4 were dialyzed overnight in a buffer containing 25 mM Tris pH 8.0, 200 mM NaCl, and 5 mM BME. Proteins were titrated with 0.5 mM palbociclib dissolved in the same buffer. For measurement of p27 ($p27^{KID}$; 25-93) binding to GST-CDK4, proteins were eluted in separate runs from a Superdex 200 column equilibrated in a buffer containing 25 mM Tris pH 8.0, 200 mM NaCl, and 5 mM BME. 250 μM p27 was titrated into 40 μM GST-CDK4 in the absence and presence of 50 μM palbociclib.

Supplementary Material

Refer to Web version on PubMed Central for supplementary material.

Acknowledgments:

Funding: This research was supported by grants from the NIH to E.S.K. and A.K.W. (R01CA211878), K.M.S. (R01 CA190408 and U01 CA19924), and S.M.R. (R01 GM124148 and R01 CA228413), from the Tobacco-Related Disease Research Program of the University of California, Grant Number 28IR-0046, to S.M.R., and from the Samuel Waxman Cancer Research Foundation to K.M.S.. K.Z.G. (F31 CA206244) and K.L. (F30 CA239476) are supported by fellowships from the NIH. Data collection at the ALS Beamline 8.3.1 is supported by the UC Office of the President, Multicampus Research Programs and Initiatives Grant MR-15-328599 and Program for Breakthrough Biomedical Research, which is partially funded by the Sandler Foundation.

References:

1. Hunter T, Pines J, Cyclins and cancer. II: Cyclin D and CDK inhibitors come of age. Cell 79, 573–582 (1994). [PubMed: 7954824]
2. Sherr CJ, Cancer cell cycles. Science 274, 1672–1677 (1996). [PubMed: 8939849]
3. Malumbres M, Cyclin-dependent kinases. Genome Biol 15, 122 (2014). [PubMed: 25180339]
4. Otto T, Sicinski P, Cell cycle proteins as promising targets in cancer therapy. Nat Rev Cancer 17, 93–115 (2017). [PubMed: 28127048]
5. Sherr CJ, Beach D, Shapiro GI, Targeting CDK4 and CDK6: From Discovery to Therapy. Cancer Discov 6, 353–367 (2016). [PubMed: 26658964]
6. Weinberg RA, The retinoblastoma protein and cell cycle control. Cell 81, 323–330 (1995). [PubMed: 7736585]
7. Finn RS et al. , Palbociclib and Letrozole in Advanced Breast Cancer. N Engl J Med 375, 1925–1936 (2016). [PubMed: 27959613]
8. Finn RS et al. , The cyclin-dependent kinase 4/6 inhibitor palbociclib in combination with letrozole versus letrozole alone as first-line treatment of oestrogen receptor-positive, HER2-negative, advanced breast cancer (PALOMA-1/TRIO-18): a randomised phase 2 study. Lancet Oncol 16, 25–35 (2015). [PubMed: 25524798]
9. Jeffrey PD et al. , Mechanism of CDK activation revealed by the structure of a cyclinA-CDK2 complex. Nature 376, 313–320 (1995). [PubMed: 7630397]
10. Day PJ et al. , Crystal structure of human CDK4 in complex with a D-type cyclin. Proceedings of the National Academy of Sciences 106, 4166–4170 (2009).
11. Takaki T et al. , The structure of CDK4/cyclin D3 has implications for models of CDK activation. Proceedings of the National Academy of Sciences of the United States of America 106, 4171–4176 (2009). [PubMed: 19237555]
12. Matsushime H et al. , Identification and properties of an atypical catalytic subunit (p34PSK-J3/cdk4) for mammalian D type G1 cyclins. Cell 71, 323–334 (1992). [PubMed: 1423597]

13. Anders L et al. , A Systematic Screen for CDK4/6 Substrates Links FOXM1 Phosphorylation to Senescence Suppression in Cancer Cells. Cancer Cell 20, 620–634 (2011). [PubMed: 22094256]
14. Kitagawa M et al. , The consensus motif for phosphorylation by cyclin D1-Cdk4 is different from that for phosphorylation by cyclin A/E-Cdk2. The EMBO Journal 15, 7060–7069 (1996). [PubMed: 9003781]
15. Konstantinidis K, Radhakrishnan R, Gu F, Rao RN, Yeh WK, Purification, characterization, and kinetic mechanism of cyclin D1. CDK4, a major target for cell cycle regulation. The Journal of biological chemistry 273, 26506–26515 (1998). [PubMed: 9756886]
16. Knight ZA, Shokat KM, Features of selective kinase inhibitors. Chemistry and Biology 12, 621–637 (2005). [PubMed: 15975507]
17. Pan W, Cox S, Hoess RH, Grafstrom RH, A cyclin D1/cyclin-dependent kinase 4 binding site within the C domain of the retinoblastoma protein. Cancer Res 61, 2885–2891 (2001). [PubMed: 11306463]
18. Topacio BR et al. , Cyclin D-Cdk4,6 Drives Cell-Cycle Progression via the Retinoblastoma Protein's C-Terminal Helix. Mol Cell 74, 758–770 (2019). [PubMed: 30982746]
19. Verba KA et al. , Atomic structure of Hsp90-Cdc37-Cdk4 reveals that Hsp90 traps and stabilizes an unfolded kinase. Science (New York, N.Y.) 352, 1542–1547 (2016).
20. Hallett ST et al. , Differential Regulation of G1 CDK Complexes by the Hsp90-Cdc37 Chaperone System. Cell Rep 21, 1386–1398 (2017). [PubMed: 29091774]
21. Brotherton DH et al. , Crystal structure of the complex of the cyclin D-dependent kinase Cdk6 bound to the cell-cycle inhibitor p19INK4d. Nature 395, 244–250 (1998). [PubMed: 9751051]
22. Russo AA, Tong L, Lee J-O, Jeffrey PD, Pavletich NP, Structural basis for inhibition of the cyclin-dependent kinase Cdk6 by the tumour suppressor p16 INK4a. Nature 395, 237–243 (1998). [PubMed: 9751050]
23. Matsuoka M, Kato JY, Fisher RP, Morgan DO, Sherr CJ, Activation of cyclin-dependent kinase 4 (cdk4) by mouse MO15-associated kinase. Mol Cell Biol 14, 7265–7275 (1994). [PubMed: 7935441]
24. Ray A, James MK, Larochelle S, Fisher RP, Blain SW, p27Kip1 inhibits cyclin D-cyclin-dependent kinase 4 by two independent modes. Mol Cell Biol 29, 986–999 (2009). [PubMed: 19075005]
25. Sherr CJ, Roberts JM, CDK inhibitors: positive and negative regulators of G1-phase progression. Genes Dev 13, 1501–1512 (1999). [PubMed: 10385618]
26. Lacy ER et al. , p27 binds cyclin-CDK complexes through a sequential mechanism involving binding-induced protein folding. Nat Struct Mol Biol 11, 358–364 (2004). [PubMed: 15024385]
27. Martín-caballero J et al. , Tumor Susceptibility of p21 Waf1 / Cip1 -deficient Mice. Cancer Research 61, 6234–6238 (2001). [PubMed: 11507077]
28. Fero ML et al. , A syndrome of multiorgan hyperplasia with features of gigantism, tumorigenesis, and female sterility in p27Kip1-deficient Mice. Cell 85, 733–744 (1996). [PubMed: 8646781]
29. Sperka T, Wang J, Rudolph KL, DNA damage checkpoints in stem cells, ageing and cancer. Nat Rev Mol Cell Biol 13, 579–590 (2012). [PubMed: 22914294]
30. Russo AA, Jeffrey PD, Patten AK, Massagué J, Pavletich NP, Crystal structure of the p27(Kip1) cyclin-dependent-kinase inhibitor bound to the cyclin A-Cdk2 complex. Nature 382, 325–331 (1996). [PubMed: 8684460]
31. Cheng M et al. , The p21(Cip1) and p27(Kip1) CDK 'inhibitors' are essential activators of cyclin D-dependent kinases in murine fibroblasts. EMBO J 18, 1571–1583 (1999). [PubMed: 10075928]
32. Blain SW, Montalvo E, Massagué J, Differential interaction of the cyclin-dependent kinase (CDK) inhibitor p27(Kip1) with cyclin A-Cdk2 and cyclin D2-Cdk4. Journal of Biological Chemistry 272, 25863–25872 (1997).
33. Soos TJ et al. , Formation of p27-CDK complexes during the human mitotic cell cycle. Cell Growth Differ 7, 135–146 (1996). [PubMed: 8822197]
34. James MK, Ray A, Leznova D, Blain SW, Differential modification of p27Kip1 controls its cyclin D-cdk4 inhibitory activity. Molecular and cellular biology 28, 498–510 (2008). [PubMed: 17908796]

35. Larrea MD et al. , Phosphorylation of p27Kip1 regulates assembly and activation of cyclin D1-Cdk4. Mol Cell Biol 28, 6462–6472 (2008). [PubMed: 18710949]
36. McConnell BB, Gregory FJ, Stott FJ, Hara E, Peters G, Induced expression of p16(INK4a) inhibits both CDK4- and CDK2-associated kinase activity by reassortment of cyclin-CDK-inhibitor complexes. Mol Cell Biol 19, 1981–1989 (1999). [PubMed: 10022885]
37. LaBaer J et al. , New functional actvities for the p21 family of CDK inhibitors. Genes and Development 11, 847–862 (1997). [PubMed: 9106657]
38. Patel P et al. , Brk/Protein Tyrosine Kinase 6 Phosphorylates p27 KIP1 , Regulating the Activity of Cyclin D–Cyclin-Dependent Kinase 4. Molecular and Cellular Biology 35, 1506–1522 (2015). [PubMed: 25733683]
39. Brown NR, Noble ME, Endicott JA, Johnson LN, The structural basis for specificity of substrate and recruitment peptides for cyclin-dependent kinases. Nat Cell Biol 1, 438–443 (1999). [PubMed: 10559988]
40. Schulman BA, Lindstrom DL, Harlow E, Substrate recruitment to cyclin-dependent kinase 2 by a multipurpose docking site on cyclin A. Proc Natl Acad Sci U S A 95, 10453–10458 (1998). [PubMed: 9724724]
41. Nolen B, Taylor S, Ghosh G, Regulation of protein kinases: Controlling activity through activation segment conformation. Molecular Cell 15, 661–675 (2004). [PubMed: 15350212]
42. Wood DJ, Endicott JA, Structural insights into the functional diversity of the CDK-cyclin family. Open Biol 8, (2018).
43. Blain SW, Switching cyclin D-Cdk4 kinase activity on and off. Cell Cycle 7, 892–898 (2008). [PubMed: 18414028]
44. Tsytlonok M et al. , Dynamic anticipation by Cdk2/Cyclin A-bound p27 mediates signal integration in cell cycle regulation. Nat Commun 10, 1676 (2019). [PubMed: 30976006]
45. Grimmler M et al. , Cdk-inhibitory activity and stability of p27Kip1 are directly regulated by oncogenic tyrosine kinases. Cell 128, 269–280 (2007). [PubMed: 17254966]
46. Toogood PL et al. , Discovery of a Potent and Selective Inhibitor of Cyclin-Dependent Kinase 4 / 6. J Med Chem 4, 2388–2406 (2005).
47. Chen P et al. , Spectrum and Degree of CDK Drug Interactions Predicts Clinical Performance. Mol Cancer Ther 15, 2273–2281 (2016). [PubMed: 27496135]
48. Matsushime H et al. , D-type cyclin-dependent kinase activity in mammalian cells. Mol Cell Biol 14, 2066–2076 (1994). [PubMed: 8114738]
49. Zhao Q et al. , Broad-Spectrum Kinase Profiling in Live Cells with Lysine-Targeted Sulfonyl Fluoride Probes. J Am Chem Soc 139, 680–685 (2017). [PubMed: 28051857]
50. Polier S et al. , ATP-competitive inhibitors block protein kinase recruitment to the Hsp90-Cdc37 system. Nat Chem Biol 9, 307–312 (2013). [PubMed: 23502424]
51. Hallett ST et al. , Differential Regulation of G1 CDK Complexes by the Hsp90-Cdc37 Chaperone System. Cell Reports 21, 1386–1398 (2017). [PubMed: 29091774]
52. Green JL et al. , Direct CDKN2 Modulation of CDK4 Alters Target Engagement of CDK4 Inhibitor Drugs. Mol Cancer Ther 18, 771–779 (2019). [PubMed: 30837298]
53. Dean JL, Thangavel C, McClendon AK, Reed CA, Knudsen ES, Therapeutic CDK4/6 inhibition in breast cancer: key mechanisms of response and failure. Oncogene 29, 4018–4032 (2010). [PubMed: 20473330]
54. Wiedemeyer WR et al. , Pattern of retinoblastoma pathway inactivation dictates response to CDK4/6 inhibition in GBM. Proc Natl Acad Sci U S A 107, 11501–11506 (2010). [PubMed: 20534551]
55. Harper JW, Adami GR, Wei N, Keyomarsi K, Elledge SJ, The p21 Cdk-interacting protein Cip1 is a potent inhibitor of G1 cyclin-dependent kinases. Cell 75, 805–816 (1993). [PubMed: 8242751]
56. Kato A, Takahashi H, Takahashi Y, Matsushime H, Inactivation of the cyclin D-dependent kinase in the rat fibroblast cell line, 3Y1, induced by contact inhibition. J Biol Chem 272, 8065–8070 (1997). [PubMed: 9065480]
57. Ladha MH, Lee KY, Upton TM, Reed MF, Ewen ME, Regulation of exit from quiescence by p27 and cyclin D1-CDK4. Mol Cell Biol 18, 6605–6615 (1998). [PubMed: 9774675]

58. Toyoshima H, Hunter T, p27, a novel inhibitor of G1 cyclin-Cdk protein kinase activity, is related to p21. Cell 78, 67–74 (1994). [PubMed: 8033213]
59. Polyak K et al. , p27Kip1, a cyclin-Cdk inhibitor, links transforming growth factor-beta and contact inhibition to cell cycle arrest. Genes Dev 8, 9–22 (1994). [PubMed: 8288131]
60. Zhang H, Hannon GJ, Beach D, p21-containing cyclin kinases exist in both active and inactive states. Genes Dev 8, 1750–1758 (1994). [PubMed: 7958854]
61. Wang H et al. , The metabolic function of cyclin D3-CDK6 kinase in cancer cell survival. Nature 546, 426–430 (2017). [PubMed: 28607489]
62. Zhang J et al. , Cyclin D-CDK4 kinase destabilizes PD-L1 via cullin 3-SPOP to control cancer immune surveillance. Nature 553, 91–95 (2018). [PubMed: 29160310]
63. Zhao B, Burgess K, PROTACs suppression of CDK4/6, crucial kinases for cell cycle regulation in cancer. Chem Commun (Camb) 55, 2704–2707 (2019). [PubMed: 30758029]
64. Schade AE, Oser MG, Nicholson HE, DeCaprio JA, Cyclin D-CDK4 relieves cooperative repression of proliferation and cell cycle gene expression by DREAM and RB. Oncogene, (2019).
65. Ramsey MR et al. , Expression of p16Ink4a compensates for p18Ink4c loss in cyclin-dependent kinase 4/6-dependent tumors and tissues. Cancer Res 67, 4732–4741 (2007). [PubMed: 17510401]
66. Young RJ et al. , Loss of CDKN2A expression is a frequent event in primary invasive melanoma and correlates with sensitivity to the CDK4/6 inhibitor PD0332991 in melanoma cell lines. Pigment Cell Melanoma Res 27, 590–600 (2014). [PubMed: 24495407]
67. Jiang H, Chou HS, Zhu L, Requirement of cyclin E-Cdk2 inhibition in p16(INK4a)-mediated growth suppression. Mol Cell Biol 18, 5284–5290 (1998). [PubMed: 9710613]
68. Reynisdottir I, Polyak K, Iavarone A, Massague J, Kip/Cip and Ink4 Cdk inhibitors cooperate to induce cell cycle arrest in response to TGF-beta. Genes Dev 9, 1831–1845 (1995). [PubMed: 7649471]
69. Moser J, Miller I, Carter D, Spencer SL, Control of the Restriction Point by Rb and p21. Proc Natl Acad Sci U S A 115, E8219–E8227 (2018). [PubMed: 30111539]
70. Novotny CJ et al. , Overcoming resistance to HER2 inhibitors through state-specific kinase binding. Nat Chem Biol 12, 923–930 (2016). [PubMed: 27595329]
71. Schindler T et al. , Structural mechanism for STI-571 inhibition of abelson tyrosine kinase. Science 289, 1938–1942 (2000). [PubMed: 10988075]
72. McGrath DA et al. , Structural basis of divergent cyclin-dependent kinase activation by Spy1/RINGO proteins. EMBO J 36, 2251–2262 (2017). [PubMed: 28666995]
73. Leslie AG, The integration of macromolecular diffraction data. Acta Crystallogr D Biol Crystallogr 62, 48–57 (2006). [PubMed: 16369093]
74. Bailey S, The Ccp4 Suite - Programs for Protein Crystallography. Acta Crystallographica Section D-Biological Crystallography 50, 760–763 (1994).
75. Evans P, Scaling and assessment of data quality. Acta Crystallogr D Biol Crystallogr 62, 72–82 (2006). [PubMed: 16369096]
76. McCoy AJ et al. , Phaser crystallographic software. J Appl Crystallogr 40, 658–674 (2007). [PubMed: 19461840]
77. Emsley P, Cowtan K, Coot: model-building tools for molecular graphics. Acta Crystallogr D Biol Crystallogr 60, 2126–2132 (2004). [PubMed: 15572765]
78. Adams PD et al. , PHENIX: a comprehensive Python-based system for macromolecular structure solution. Acta Crystallogr D Biol Crystallogr 66, 213–221 (2010). [PubMed: 20124702]
79. Ou L et al. , Incomplete folding upon binding mediates Cdk4/cyclin D complex activation by tyrosine phosphorylation of inhibitor p27 protein. Journal of Biological Chemistry 286, 30142–30151 (2011).

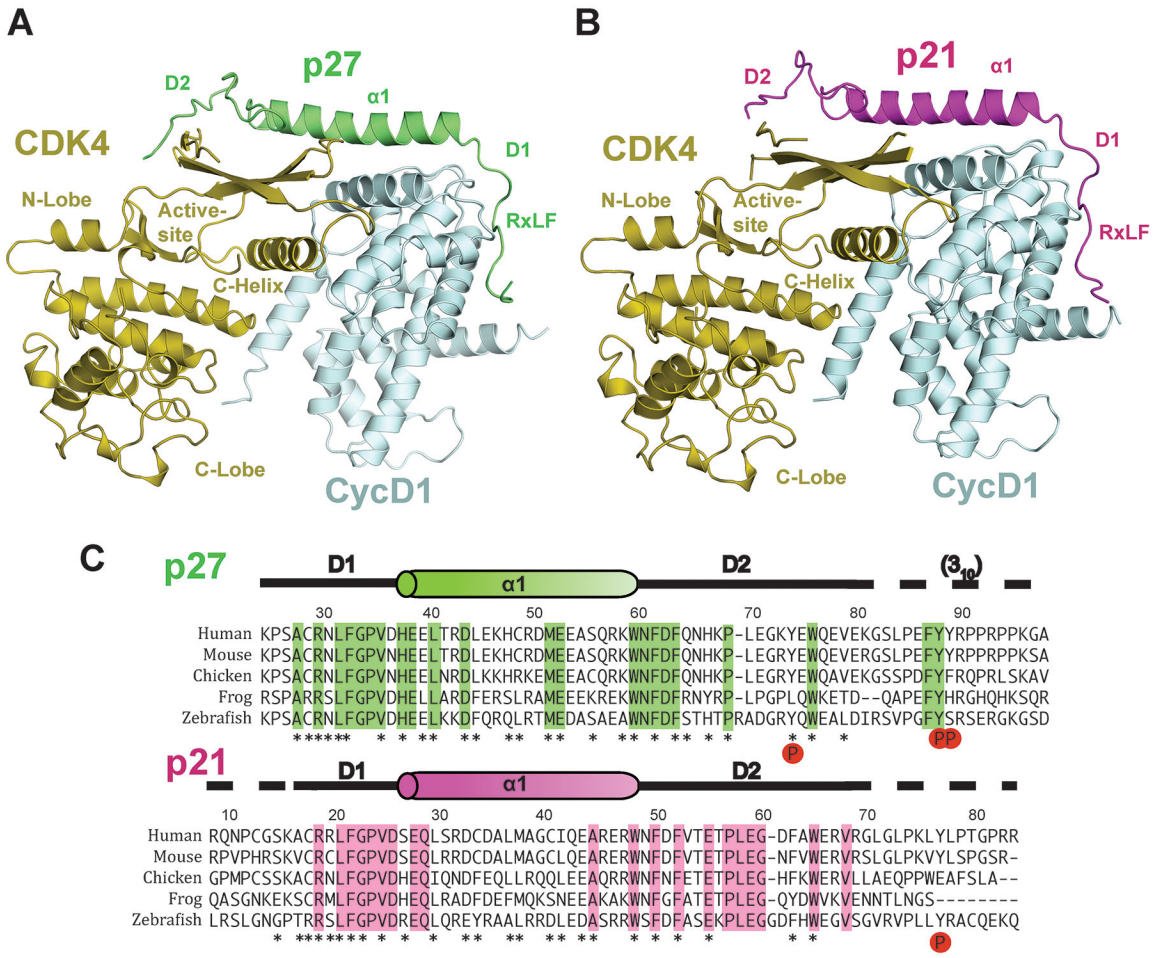

Fig. 1: Structures of the p27-CDK4-CycD1 and p21-CDK4-CycD1 complexes.

(A) Overall structure of p27-CDK4-CycD1. p27 (green) binds CycD1 (cyan) with its D1 domain and CDK4 (gold) with its D2 domain. **(B)** Structure of p21-CDK4-CycD1. p21 (magenta) adopts a similar fold to p27, bridging CDK4 (gold) and CycD1 (cyan). **(C)** Sequence alignment of p27 and p21. Asterisks represent residues directly interacting with CDK4 or CycD1. The known tyrosine phosphorylation sites are noted. Secondary structure observed in the crystal is indicated above the sequences. Dashed lines indicate sequences in the crystallized protein that are not visible in the electron density, including the C-terminal sequence in p27 that forms a 3_{10} helix when bound to CDK2 (in parentheses).

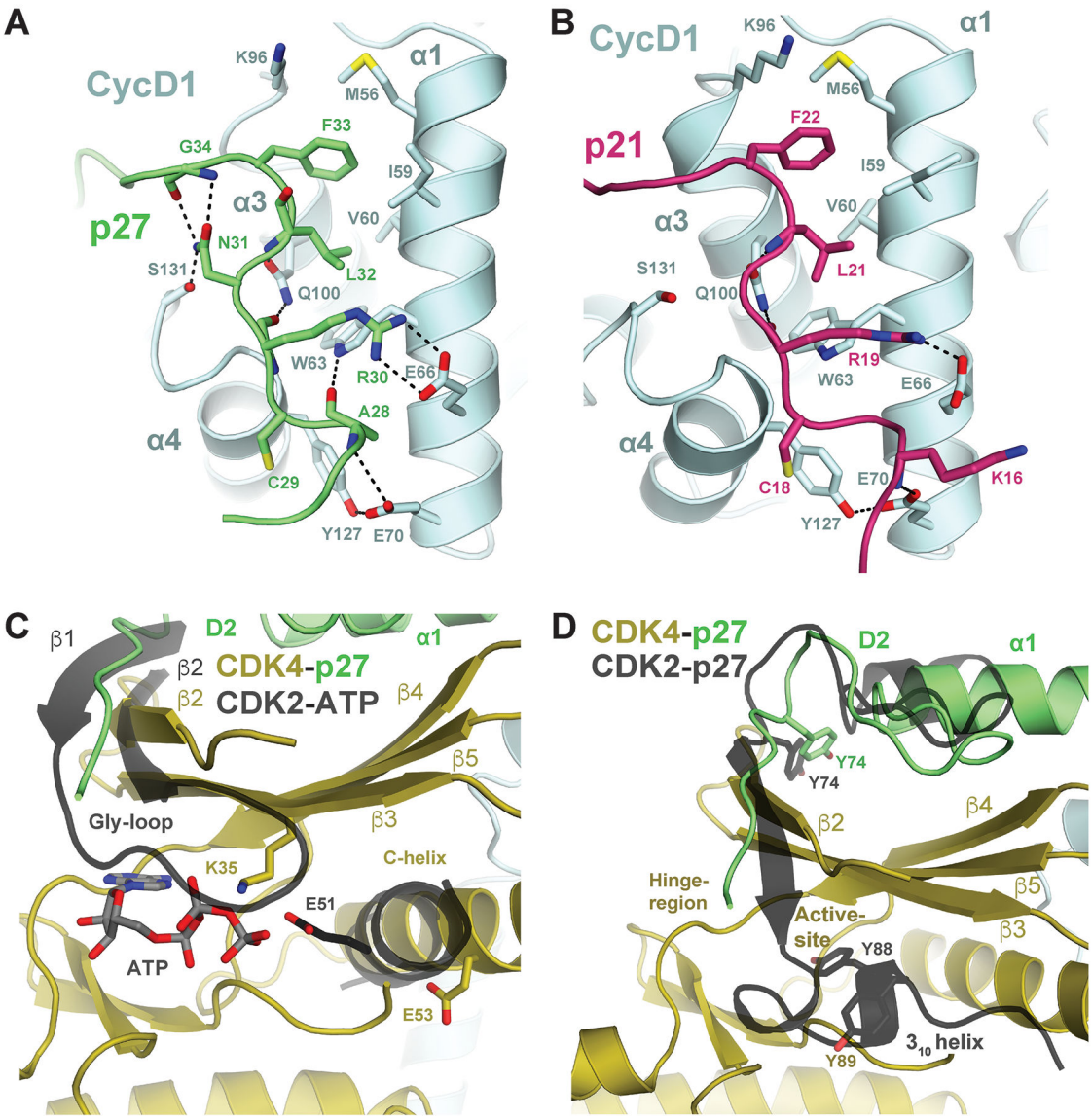

Fig. 2: p27 and p21 inhibit substrate binding and catalytic activity.

(**A)** Association between the p27 RxLF motif (green) and the MVRIL cleft in CycD1 (cyan) competes for substrate docking. (**B**) The p21 RxLF (magenta) bound to CycD1 (cyan). (**C)** Binding of the D2 region in p27 (green) displaces the β1 strand in the CDK4 N-lobe (gold), disrupting the ATP-binding site. The structure shown in grey for comparison, including the ATP, is from CDK2 in the active CDK2-CycA dimer. The CDK4 β1 strand and following Gly-loop are not visible in the p27-CDK4-CycD1 trimer structure, indicating they are disordered. The C-helix remains in an inactive conformation in the CDK4-p27 structure. (**D**) Comparison of binding of p27 to CDK2 (p27 in grey) and to CDK4 (p27 in green, CDK4 in gold). The 3_{10} helix in p27 that binds the CDK2 ATP-site is not visible and likely remains disordered upon CDK4 binding. Tyrosine phosphorylation sites are shown.

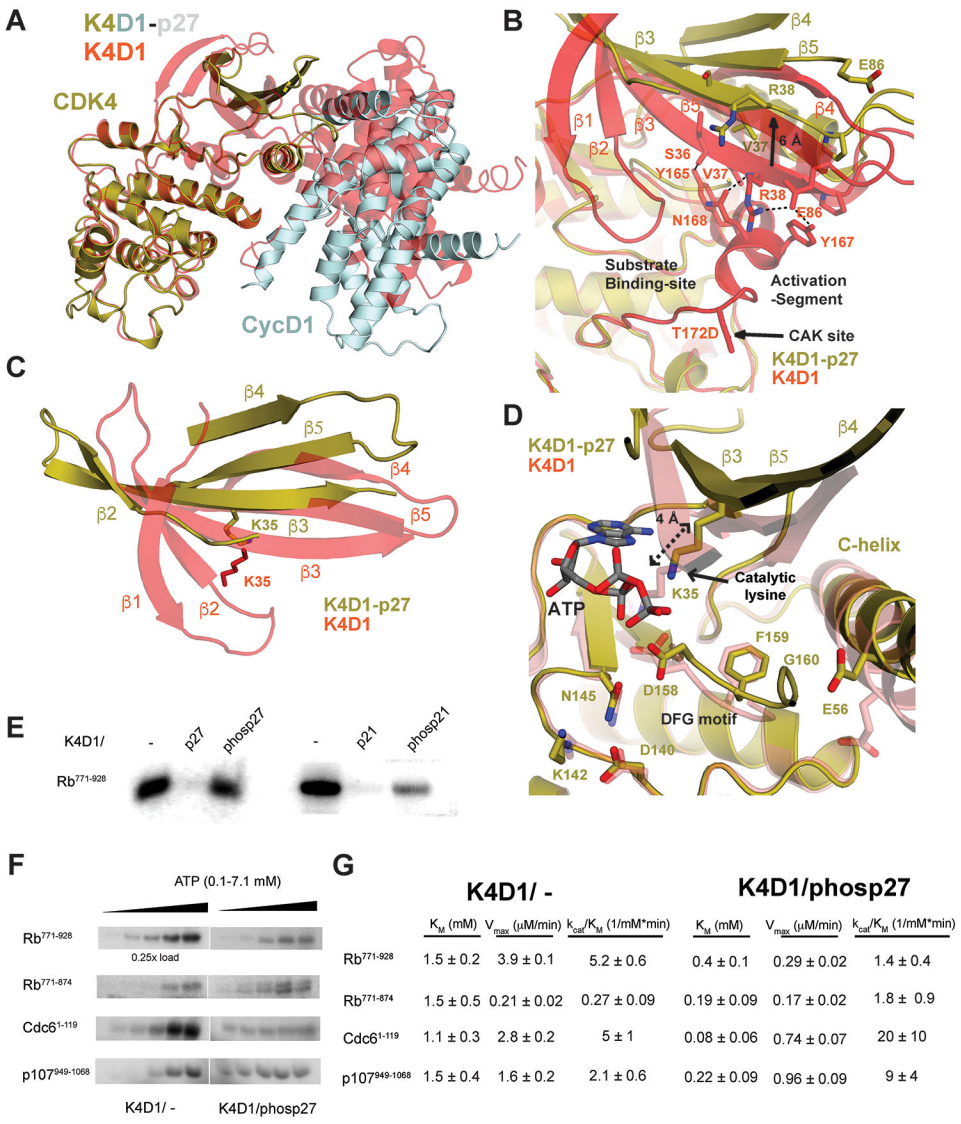

	K4D1/ -			K4D1/phosp27		
	K_M (mM)	V_{max} (μM/min)	k_{cat}/K_M (1/mM*min)	K_M (mM)	V_{max} (μM/min)	k_{cat}/K_M (1/mM*min)
$Rb^{771-928}$	1.5 ± 0.2	3.9 ± 0.1	5.2 ± 0.6	0.4 ± 0.1	0.29 ± 0.02	1.4 ± 0.4
$Rb^{771-874}$	1.5 ± 0.5	0.21 ± 0.02	0.27 ± 0.09	0.19 ± 0.09	0.17 ± 0.02	1.8 ± 0.9
$Cdc6^{1-119}$	1.1 ± 0.3	2.8 ± 0.2	5 ± 1	0.08 ± 0.06	0.74 ± 0.07	20 ± 10
$p107^{949-1068}$	1.5 ± 0.4	1.6 ± 0.2	2.1 ± 0.6	0.22 ± 0.09	0.96 ± 0.09	9 ± 4

Fig. 3: p27 induces structural changes that promote ATP coordination and processing.

(A-D) Structural alignment of CDK4-CycD1 with p27 (gold-cyan) and without p27 (red, PDB code: 2W96) reveals movement of both the CDK4 N-lobe and CycD1 domains relative to the CDK4 C-lobe. **(E)** Phosphorylation of purified $Rb^{771-928}$ with ^{32}P-ATP and the indicated dimer (K4D1/−) or trimer complex. **(F-G)** Steady state kinase assays measuring effects of ATP concentration on initial reaction rate, measured by incorporation of ^{32}P-ATP. Reactions include CDK4 dimer (K4D1/−) or active trimer (K4D1/phosp27) and the indicated substrate.

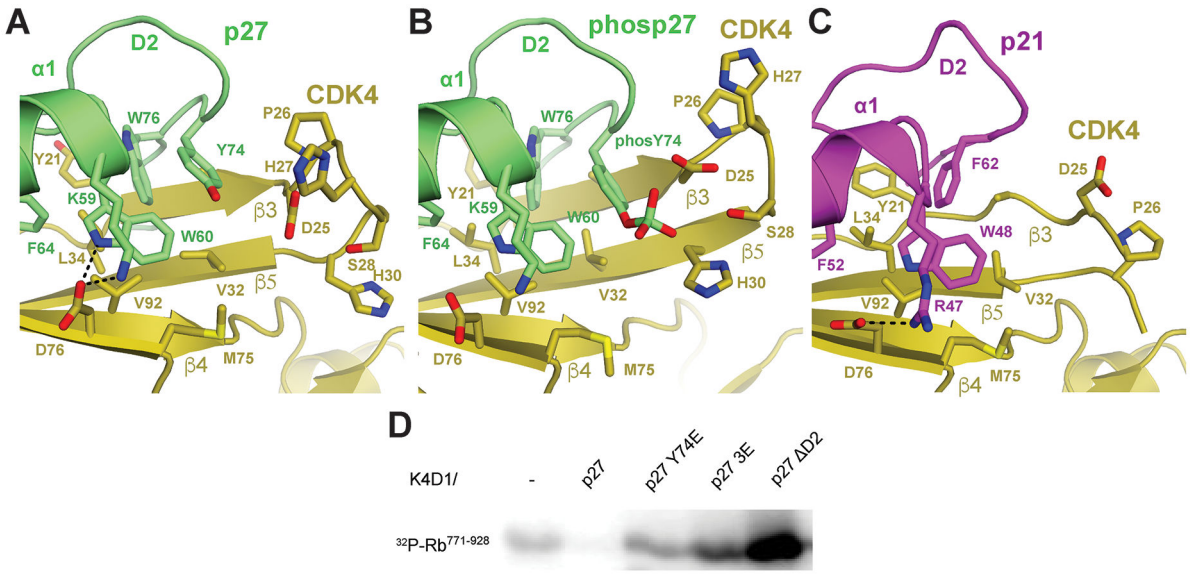

Fig. 4: Y74 phosphorylation disrupts the p27 D2-CDK4 interface.

Comparison of CDK4-CycD1 structures with **(A)** unphosphorylated p27, **(B)** phosphorylated p27, and **(C)** p21. **(D)** ^{32}P-ATP phosphorylation of Rb$^{771-928}$ using K4D1 dimer or trimer enzymes assembled with the indicted p27 kinase inhibitory domain construct (residues 25-93). 3E contains three glutamate phosphomimetics at Y74, Y88 and Y89. ΔD2 contains p27 residues 25-60, and therefore lacks the D2 CDK4-binding domain

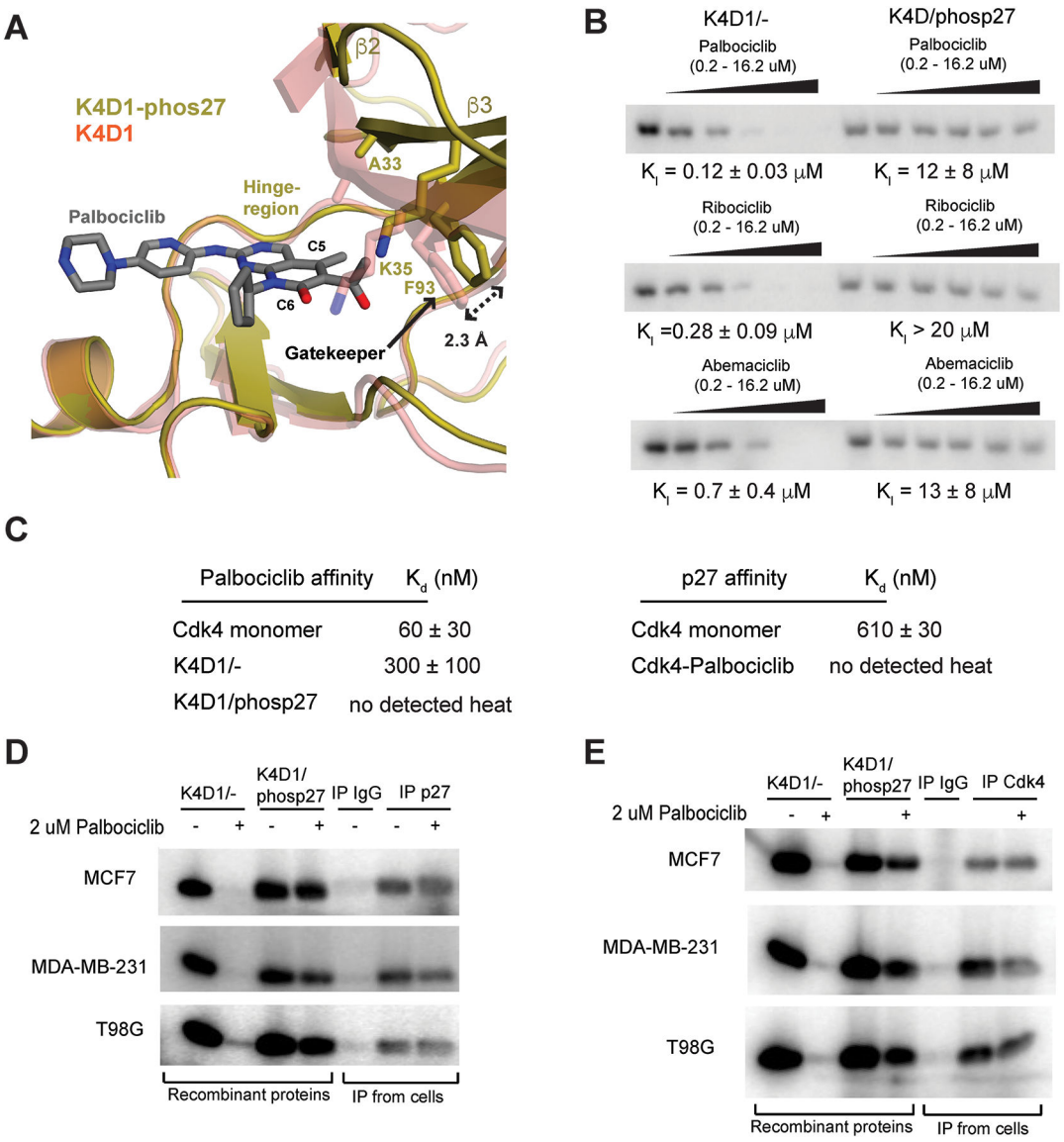

Fig. 5: Palbociclib does not bind and poorly inhibits purified and endogenous CDK4 trimer complexes.

(A) K4D1 dimer (PDB ID: 2W96) and the phosp27-K4D1 trimer structures were aligned with palbociclib-bound CDK6 (PDB ID: 2EUF, not shown) to model the position and interactions of the drug when bound to CDK4. **(B)** ^{32}P-ATP phosphorylation of Rb$^{771-928}$ using CDK4-CycD1 dimer (K4D1/−) and phosp27-CDK4-CycD1 trimer (K4D1/phosp27) enzymes in the absence (left most lane in each titration) and presence of increasing inhibitor concentrations (see Fig. S8A for quantification). Each drug is dosed from 0.2 μM to 16.2 μM in 3-fold increments. **(C)** ITC affinities for palbociclib (left) or p27 (right) titrated into the indicated enzyme. (**D**) The indicated cell lysates were immunoprecipitated with control or with p27 antibody, and the activity of the immunoprecipitate was used to phosphorylate Rb$^{771-928}$ with ^{32}P-ATP in the absence or presence of palbociclib. Reactions with the indicated recombinant dimer (K4D1/−) or trimer (K4D1/phosp27) enzymes are shown for

comparison in the first four lanes. **(E)** As in panel **D,** except lysates were precipitated with antiserum raised against a CDK4 C-terminal peptide.

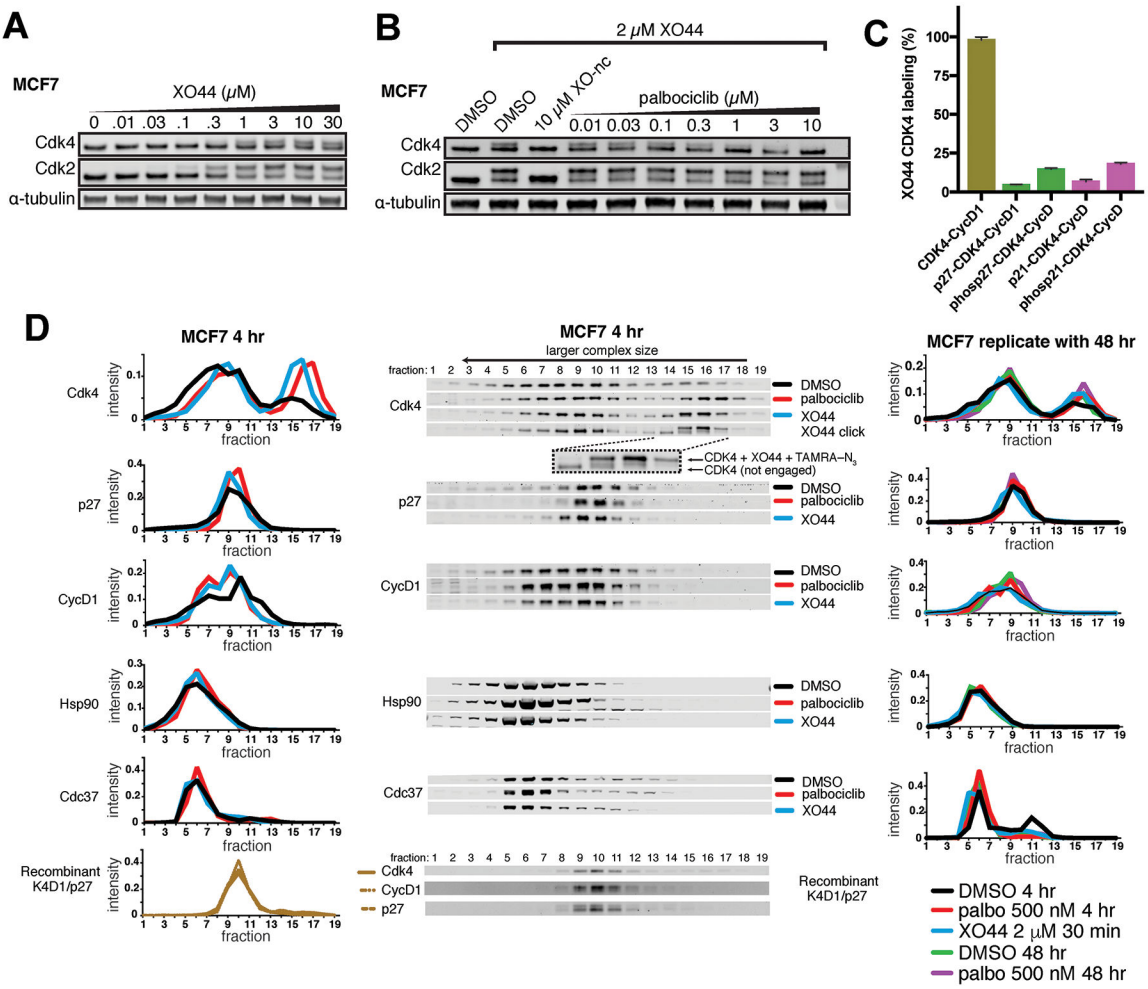

Fig. 6: The ATP-site occupancy probe XO44 labels monomer CDK4 in MCF7 cells.

(A) Labeling of endogenous CDK4 and CDK2 by the promiscuous covalent ATP-site probe XO44. MCF7 cells were treated with DMSO vehicle or XO44 at the indicated concentrations for 30 min. Lysates were subjected to click reaction with TAMRA–azide to visualize XO44 labeling of proteins by gel mobility shift. **(B)** Palbociclib competes with XO44 for CDK4 binding but not CDK2 binding. Experiment performed as in panel **A,** but cells were pretreated for 60 mins with DMSO, a non-clickable analog of XO44 (XO-nc), or with increasing concentrations of palbociclib. (**C**) XO44 efficiently labels purified recombinant CDK4-CycD1 dimer but not trimer complexes with p21 or p27 as determined by electrospray ionization mass spectrometry. Protein complexes were treated with DMSO or XO44. Average percent labeling was determined for three replicates with standard deviation shown as error bars. **(D)** Asynchronous MCF7 cells were treated with DMSO, XO44 (2 μM, 30 min) or palbociclib (500 nM, 4 hr), and lysates were fractionated using Superdex200 size-exclusion chromatography. XO44 labeling was monitored by gel mobility shift after click reaction with TAMRA–N_3 (“XO44 click”). Normalized quantification of band signals from the western blots using the indicated antibody are shown. A benchmark chromatography experiment using the recombinant protein complex is displayed at the bottom of the panel. See Fig. S10 for data using MDA-MB-231 cells.

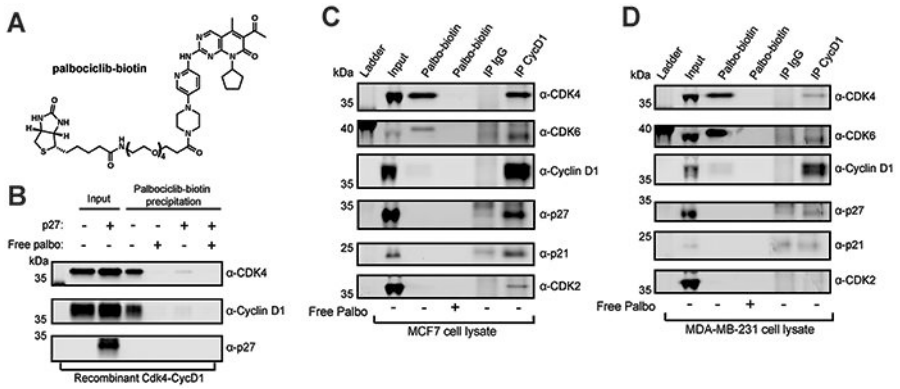

Fig. 7: Palbociclib directly targets CDK4/6 monomer in cell lysate.

(**A**) Chemical structure of palbociclib-biotin synthesized here. (**B**) Palbociclib-biotin precipitated purified recombinant CDK4-CycD1 dimer, but not p27-CDK4-CycD1 trimer. (**C and D**) MCF7 or MDA-MB-231 cell lysates were used in a precipitation reaction with palbociclib-biotin. A CycD1 antibody was also used to precipitate CDK4/6 from cell lysates to compare the total pool of CycD1 complexes to palbociclib-bound complexes.

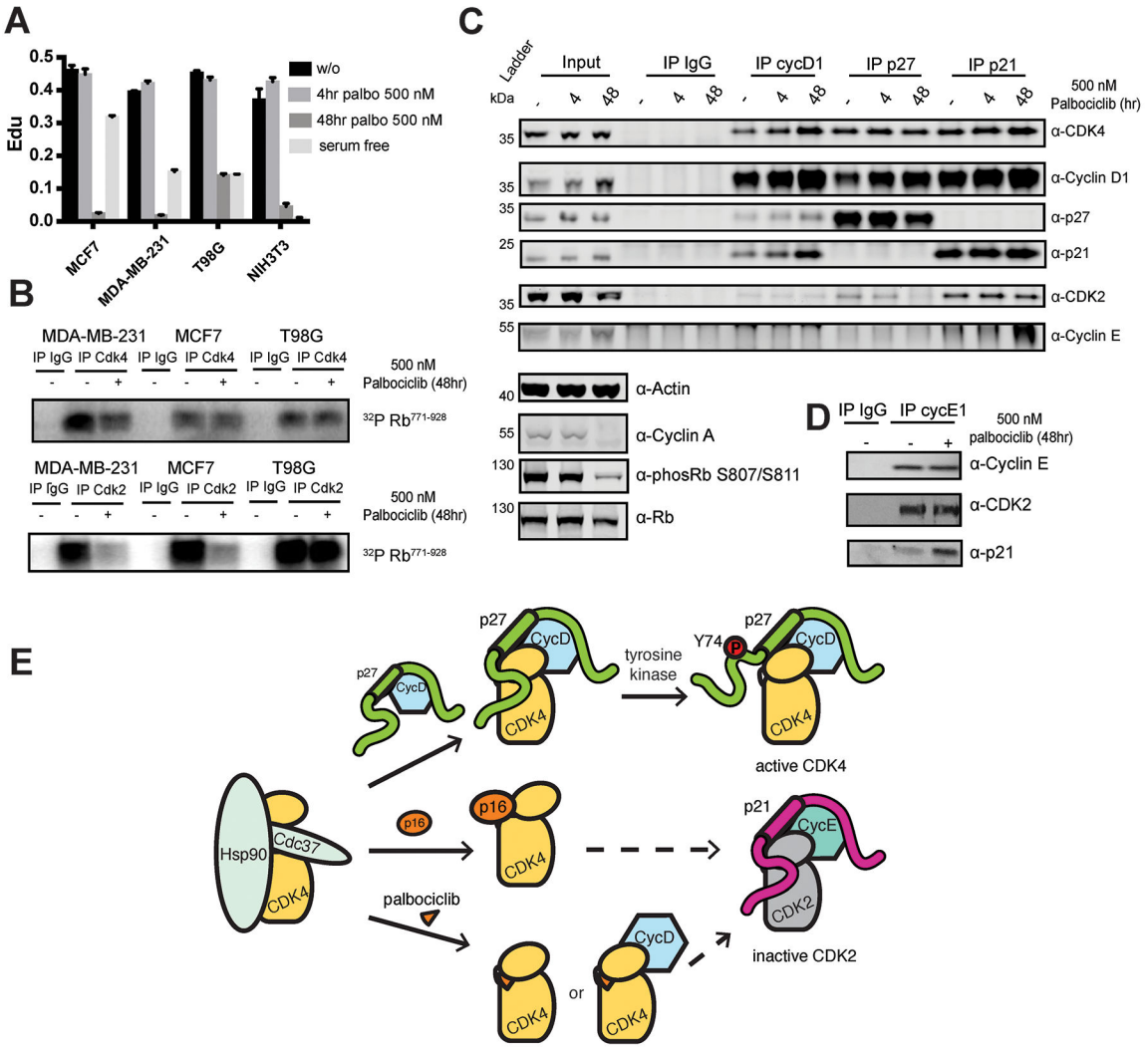

Fig. 8: Palbociclib indirectly leads to down-regulation of CDK2 through p21.

(A) Cell-cycle profiling of the cell lines used in this study upon treatment with 500 nM palbociclib for 4 or 48 hr or without drug treatment. Cells were assayed for 5-ethynyl-2-deoxyuridine (EdU) incorporation as a marker of S phase at the different time points following drug treatment. The fraction of cells showing EdU staining is reported. EdU incorporation in cells that were serum starved (serum free) for 48 hours is also shown for comparison. **(B)** Cells were treated with palbociclib as indicated for 48 hr, and lysates were immunoprecipitated with CDK4 antiserum or a CDK2 antibody. Activity of the immunoprecipitated complexes was assayed as in Fig. 5, D and E. **(C)** CycD1-, p27-, and p21-associated complexes were immunoprecipitated from MCF7 cells treated with palbociclib for the indicated time and proteins were detected by Western blot. (**D**) CycE1 was immunoprecipitated from MCF7 cells treated with palbociclib for 48 hrs. (**E**) Model for trimer assembly and CDK4 inhibition by palbociclib. Like p16 family CDK4 inhibitors, palbociclib binds monomer CDK4 and indirectly leads to inactive CDK2 complexes.

Although not observed in the breast cancer cells studied here, there may be some contexts in which palbociclib also targets CDK4 dimers.